2010 American Control Conference
Marriott Waterfront, Baltimore, MD, USA
June 30-July 02, 2010

Robust Nonlinear Control of Fuel Cell Ultra-Capacitor Hybrid System

Tahar Allag and Tuhin Das

Abstract— **In this paper we design robust control strategies for a hybrid solid oxide fuel cell ultra-capacitor system. Fuel cell control is established by using an invariant property of fuel utilization within an input-shaping framework. Two control strategies are developed. The first design uses a nonlinear control approach for which we prove the stability of the closed-loop system in presence of system uncertainties. The second uses a standard H_∞ robust control approach. Both strategies enforce the control of State of Charge (SOC) of the ultra-capacitor to a desired level. A hardware-in-the-loop test-stand is developed and experimental results are provided.**

I. INTRODUCTION

Among different fuel cell technologies, the Solid Oxide Fuel Cell (SOFC) technology has attracted significant interest in recent years. They are fuel flexible solid state devices that operate at high temperatures of (800 to 1000°C). SOFCs are fuel flexible, tolerant to impurities and hence often carry simple on-board fuel reformers. They fit well in combined heat and power (CHP) applications. An important performance variable of SOFCs is fuel utilization U, defined as the ratio of hydrogen consumption to the net available hydrogen in the anode. While high utilization implies high efficiency, very high utilization leads to reduced partial pressure of hydrogen in the fuel cell anode, which can cause irreversible damages due to anode oxidation [13]. Typically, a range of $80-90\%$ is optimum over a wide range of operating conditions [12]. In applications with significant power transients, fluctuations in U due to slow dynamic response of the fuel supply system and reformer dynamics can adversely affect stack life through fuel starvation and drastic voltage drop, [5], [17].

A majority of existing work addressing transient control of fuel cells consider the Polymer Electrolyte Membrane (PEM) fuel cell technology. Control of hybrid PEMFC systems are proposed in [1], [9], [14] and [18]. Explicit constraint handling is addressed in fewer works such as [5], [16], [17] and [19]. In comparison to PEMFC, few works on power management and control of hybrid SOFC systems appear in the literature, [8], [7]. There is increased complexity of sensing and estimation in SOFCs which is supplied with a gas mixture consisting of several species, in comparison to pure hydrogen in PEMFC. Hence measuring U requires sensing several species concentrations and flow rates leading to cost and reliability considerations, or designing observers, [2], increasing computational burden and reliance on an accurate system model.

This work was supported by the Office of Naval Research under grant #*N*000140810704

T. Allag is a graduate student and T. Das is an assistant professor of Mechanical Engineering at Rochester Institute of Technology, Rochester, NY 14623, USA, tkdeme@rit.edu

In this paper, we address the aforementioned issue through the development of a control strategy that performs feedback based regulation of the fuel cell current, in conjunction with a steady-state *invariance property* of U. The resulting deficit or surplus power delivered by the fuel cell during transients is compensated by an ultra-capacitor. The proposed fuel utilization control strategy fits directly within the overall power splitting control for the hybrid system that additionally controls the ultra-capacitor's SOC at a target value regardless of system uncertainties. Two robust control strategies are proposed in this work, a nonlinear and an H_∞ based control.

A detailed control-oriented mathematical model of an SOFC system is developed, that captures the thermodynamics, chemical kinetics, heat transfer and pressure dynamics phenomena of the fuel cell. The model has been validated against published results in [10], [13]. A system description and the uncontrolled response of U to transient current are presented in section II. Steady-state relation for this system, derived in [4], is used for open-loop control of U in section III. Feedback based input shaping of fuel cell current is presented in section IV. The hybrid fuel cell configuration and the comprehensive control designs are detailed in sections V and VI. The hardware-in-the-loop experimental test-stand is explained in VII, followed by experimental results in VIII that confirm the efficacy of our control designs. Finally concluding remarks are stated in section IX.

II. FUEL CELL SYSTEM

In this work we consider a steam reformer based tubular SOFC system. The system consists of three primary components, namely, the steam reformer, the solid oxide fuel cell and the combustor. Methane is chosen as the fuel for the system, with a molar flow rate of $\dot{N}_f$. It is noted that the control development approach in this paper can be extended to other SOFC configurations and fuels as well. The SOFC system is described in Fig.1.

The reformer produces a hydrogen-rich gas which is supplied to the anode of the fuel cell. Electrochemical reactions occurring at the anode due to current draw results in a steam-rich gas mixture at the anode exit. A fixed known fraction k of the anode exhaust is recirculated through the reformer into a mixing chamber where fuel is added. The mixing of the two fluid streams and pressurization is achieved in the gas mixer using an ejector or a recirculating fuel pump, [6]. The steam reforming process occurring in the reformer catalyst bed is an endothermic process. The energy required to sustain the process is supplied from two sources, namely, the combustor exhaust that is passed through the reformer, and the aforementioned recirculated anode flow, as shown

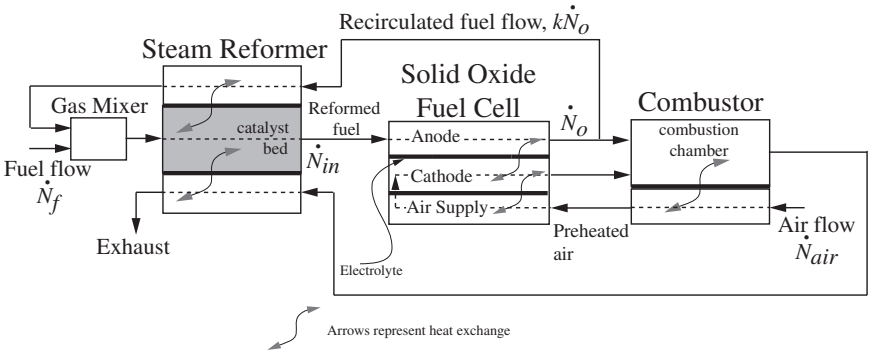

Fig. 1. Schematic Diagram of the SOFC System

in Fig.1. The remaining anode exhaust is mixed with the cathode efflux in the combustion chamber. The combustor also serves to preheat the cathode air which has a molar flow rate of $\dot{N}_{air}$. We assume our system to be comprised of $\mathscr{N}_{cell}$ tubular Solid Oxide Fuel Cells, connected in series.

Fuel utilization U is a critical indicator of the steady-state and transient performance of an SOFC system. Fuel utilization, defined as the ratio of hydrogen consumption to the hydrogen availability in the fuel cell, can be expressed mathematically as follows:

$$U = 1 - \frac{\dot{N}_o\left(4\mathscr{X}_{1,a} + \mathscr{X}_{2,a} + \mathscr{X}_{4,a}\right)}{\dot{N}_{in}\left(4\mathscr{X}_{1,r} + \mathscr{X}_{2,r} + \mathscr{X}_{4,r}\right)} \tag{1}$$

where, $\mathscr{X}_{1,a}$, $\mathscr{X}_{2,a}$, $\mathscr{X}_{4,a}$, and $\mathscr{X}_{1,r}$, $\mathscr{X}_{2,r}$, $\mathscr{X}_{4,r}$, represent the molar concentrations of CH_4, CO and H_2 in the anode and the reformer respectively, [12], [3]. U is sensitive to fuel cell current i_{fc}. This is illustrated in the simulation results presented in Fig.2. The fuel cell model is run in open loop

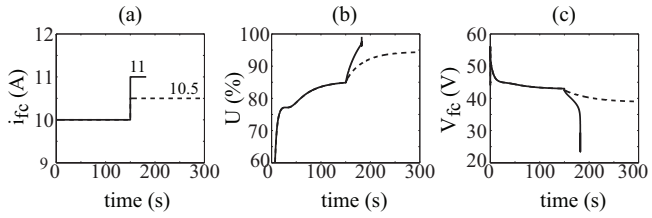

Fig. 2. Open-loop Response to Transient Current Demand

with $\mathscr{N}_{cell} = 50$, $\dot{N}_f = 7 \times 10^{-4}$moles/s and $i_{fc} = 10$A for $t < 150$s. These conditions yield a steady state utilization of $U_{ss} \approx 85\%$. Two sets of results are shown with $i_{fc} = 10.5$A and 11A for $t \geq 150$s, Fig.2(a). The resulting U is shown in Fig.2(b). The fuel cell is unable to sustain a 1A increase of current due to hydrogen starvation, manifested by $U \rightarrow 100\%$. The results show that under open-loop operation, the fuel cell is capable of responding to only small perturbations in the power demand around its operating-point. In the following sections, we use the steady-state characteristics of the fuel cell for feedback control of U.

III. OPEN-LOOP CONTROL OF U

From mass balance equations of individual species in the reformer and the anode, we obtain the following expression for steady-state utilization,

$$U_{ss} = \frac{1-k}{\left(4nF\dot{N}_f / i_{fc}\mathscr{N}_{cell}\right) - k} \tag{2}$$

For detailed analysis, see [4]. Eq.(2) is independent of internal variables such as internal flow rates, temperatures and reaction rates, etc. and is therefore an *invariant property* of U. Furthermore, since k, i_{fc} and $\dot{N}_f$ are measurable and known inputs, Eq.(2) can serve as an open-loop control to achieve a target U_{ss}. Consider the demanded fuel cell current to be $i_{fc,d}$. Then, from Eq.(2), the corresponding fuel demand $\dot{N}_{f,d}$, that satisfies a target U_{ss} is,

$$\dot{N}_{f,d} = \frac{i_{fc,d}\mathscr{N}_{cell}}{4nFU_{ss}}\left[1 - (1-U_{ss})\,k\right] \tag{3}$$

Eq.(3) only addresses steady-state behavior. Hence we must assess its effectiveness in the presence of transient current demand. Control of U using Eq.(3) is shown in Fig.3. The

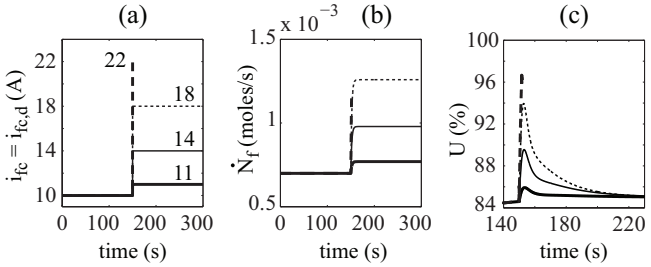

Fig. 3. Open-loop Control of U Using Eq.(3)

fuel cell system simulated is same as in Fig.2 with $i_{fc} = 10$A for $t < 150$s and target $U_{ss} = 85\%$. Four simulations are presented with $i_{fc} = 11, 14, 18$ and 22A for $t \geq 150$s, Fig.3(a). The actual fuel injected, $\dot{N}_f$, is shown in Fig.3(b). Note that while $\dot{N}_{f,d}$ changes instantaneously according to Eq.(3), $\dot{N}_f$ experiences a lag due to the dynamics of the fuel supply system that typically comprises of valves and mass flow controllers [13]. At steady-state, $\dot{N}_f = \dot{N}_{f,d}$. In this simulation, although we have assumed a first order dynamics with a time-constant of 2s, similar response is obtained with other types of fuel supply dynamics, such as ramped or rate-limited behavior. In Fig.3(c), U is plotted for individual simulations. U reaches the target $U_{ss} = 85\%$ at steady-state. The simulation abruptly ended when the step increase was

$>$ 10A. This is due to hydrogen starvation manifested by $U \rightarrow 100\%$, as seen in Fig.3(c) for step change of 12A. Note that hydrogen starvation occurred at a step increase of only 1A in the uncontrolled case, Fig.2. We make the following observations:

- In the comparison to the uncontrolled case, under open-loop control the fuel cell is capable of handling a significantly greater amount of current fluctuation.
- Under the open-loop control, U deviates from target U_{ss} during transient phase.
- Transient U is a result of the delay between a change in the fuel command $\dot{N}_{f,d}$ and its corresponding effect in the fuel cell.

Next, we propose a feedback approach that builds on the open-loop control to alleviate the transient deviation in U.

IV. FEEDBACK BASED CURRENT SHAPING

An advantage of the above approach is that U_{ss} is achieved without the knowledge of internal flow rates, temperatures, intermediate species, species concentrations or chemical reactions. However, it results in transient deviations in U. We address this issue by dynamically shaping i_{fc} using feedback. Noting that $\dot{N}_f \neq \dot{N}_{f,d}$ during transients, the actual fuel cell current i_{fc} is shaped using Eq.(2), as follows:

$$i_{fc} = \frac{4nFU_{ss}\dot{N}_f}{\mathscr{N}_{cell}} \frac{1}{[1-(1-U_{ss})k]} \tag{4}$$

Implementing Eq.(4) requires the measurement of the actual fuel flow $\dot{N}_f$, which is assumed to be available. The feedback based input shaping scheme and the open loop approach are represented in Fig.4 by the switch positions *CL* and *OL* respectively. Simulations are presented in Fig.5 to demonstrate the effect of regulating i_{fc} on transient utilization. The system simulated is the same as that in Figs.2 and 3. Referring to Fig.4, Fig.5 represents the closed-loop (CL) mode. In Fig.5, $i_{fc} = i_{fc,d} = 10$A for $t < 150$s, and $i_{fc,d} = 18, 30$ and 50A for $t \geq 150$s, and $U_{ss} = 85\%$. In response to the step changes in $i_{fc,d}$, the target fuel $\dot{N}_{f,d}$ also undergoes step changes, Figs.5(a) and (b). $\dot{N}_f$ changes according to the fuel supply dynamics which is assumed to be first order with a time constant of 2s Fig.5(b), as in the previous simulations. The regulated i_{fc} is computed using Eq.(4) and is shown in Fig.5(a). The resulting transient U is shown in Fig.5(c).

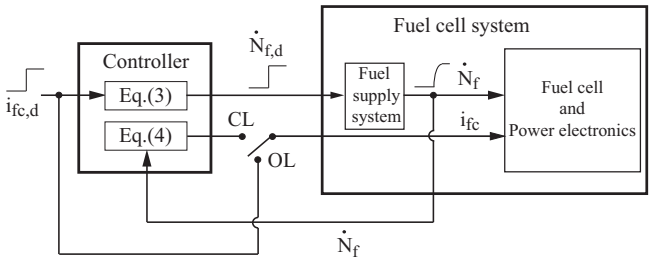

Fig. 4. Scheme for Transient Utilization Control

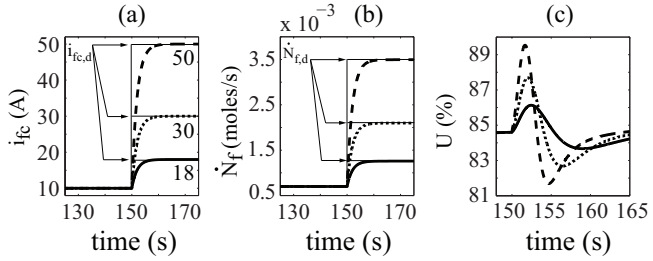

Fig. 5. Effect of Shaping i_{fc} on Transient U

It is evident from the results above that the feedback based shaping of i_{fc} drastically reduces transient U. It is also clear that this regulation increases transient current handling capability of the fuel cell by a considerable margin. Although in sections III and IV we assumed a first order fuel-supply dynamics, the observations made are applicable to a wide variety of dynamic responses [4].

V. HYBRID FUEL CELL CONFIGURATION

Dynamic regulation of i_{fc} will lead to a mismatch between the demanded power and fuel cell delivered power during transients. This mismatch can be compensated by a storage device that discharges and charges when compensating for deficit and excess power respectively. A schematic diagram of a hybrid fuel cell system is shown in Fig.6. The hybrid system consists of a fuel cell and an ultra-capacitor connected to an electrical bus through DC/DC converters. In the following sections we develop strategies for combined control of the SOFC ultra-capacitor hybrid system. The objectives of the control strategy are first, to control fuel utilization and second, to control SOC of the ultra-capacitor, at their respective target values. Within these constraints, we wish to achieve load following in the presence of rapid load transients.

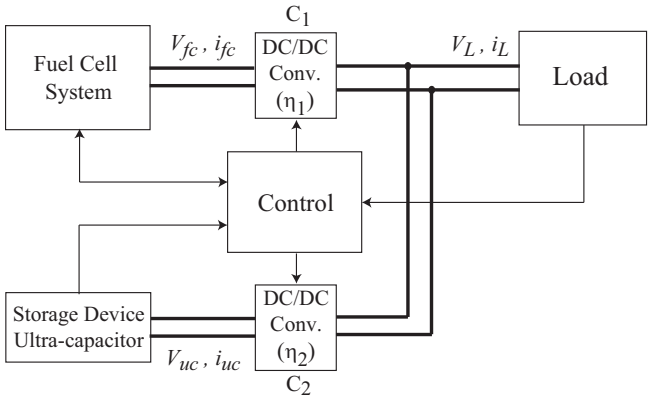

Fig. 6. Hybrid Fuel Cell System

In the control development, we make the assumption that the DC/DC converters can be treated as static power conversion devices. This leads to the following instantaneous power balance equation, developed using Fig.6

$$V_L i_L = \eta_1 V_{fc} i_{fc} + \eta_2 V_{uc} i_{uc} \tag{5}$$

where, η_1 and η_2 are the efficiencies of the power converters C_1 and C_2 respectively. The following aspects are also considered in the control development:

- Among the two DC/DC converters shown in Fig.6, C_1 operates in voltage control mode and C_2 in the current control mode. In particular, C_1 maintains a constant bus voltage and C_2 follows the commanded ultra-capacitor current $i_{uc,c}$, (we treat $i_{uc} = i_{uc,c}$).
- The ultra-capacitor current i_{uc} and the fuel demand $\dot{N}_{f,d}$ are treated as control inputs.
- Measurements of V_{fc}, V_{uc}, i_L and i_{fc}, are available.
- The DC/DC converter efficiencies η_1 and η_2 vary with operating conditions and are treated as unknowns with constant estimates $\bar{\eta}_1$ and $\bar{\eta}_2$.

VI. CONTROL DESIGN

A. Nonlinear Robust Control

A schematic diagram of the control strategy incorporating the current regulation algorithm of Fig.4 is provided in Fig.7. The fuel cell serves as the primary power source and the ultra-capacitor supplies transient demands. This, along with the objective of controlling the ultra-capacitor SOC prompts the following design of fuel cell current demand

$$i_{fc,d} = \frac{V_L i_L}{\bar{\eta}_1 V_{fc}} + g(E_s) + \delta_1, \quad E_s = S - S_t, \quad S = \frac{V_{uc}}{V_{max}} \tag{6}$$

where S is the instantaneous SOC, S_t is the target SOC and V_{max} is the maximum ultra-capacitor voltage. The function $g(E_s)$ and the robustness term δ_1 will be designed in the ensuing analysis. The fuel demand, $\dot{N}_{f,d}$, is an algebraic function of $i_{fc,d}$, given by Eq.(3), that satisfies the target utilization criterion. The target fuel cell current, $i_{fc,t}$, is based on $\dot{N}_f$ as shown in Fig.7, and is computed using Eq.(4) as

$$i_{fc,t} = \frac{4nFU_{ss}\dot{N}_f}{\mathscr{N}_{cell}} \frac{1}{[1-(1-U_{ss})k]} \tag{7}$$

The fuel cell target current $i_{fc,t}$ is indirectly achieved through the ultra-capacitor current command as follows

$$i_{uc} = i_{uc,c} = \frac{V_L i_L - \bar{\eta}_1 V_{fc} i_{fc,t}}{\bar{\eta}_2 V_{uc}} + h\left(E_{fc}\right) + \delta_2,\ E_{fc} = i_{fc} - i_{fc,t} \tag{8}$$

where the function $h\left(E_{fc}\right)$ and the robustness term δ_2 will be designed in the ensuing analysis.

Note that the current regulation approach detailed in section IV does not require any knowledge of the dynamics of the fuel supply system. However, in developing a comprehensive control strategy we assume a stability characteristics of the fuel supply system. Specifically, we consider the error variable $E_{fl} = \dot{N}_f - \dot{N}_{f,d}$ to show an exponentially stable property, i.e.

$$\left|E_{fl}(t)\right| \leq \gamma \left|E_{fl}(0)\right| e^{-\alpha t}, \quad \gamma, \alpha > 0 \tag{9}$$

where, γ and α are unknown but their upper and lower bounds respectively exist and can be estimated. This is not a restrictive condition, since any stable linear n^{th} order behavior or nonlinear behaviors such as ramped response or rate limited response can be bounded by an exponential decay within a limit of accuracy. From Eqs.(3) and (7), it is evident that Eq.(9) implies

$$\left|E_{fc,t}(t)\right| \leq \gamma \left|E_{fc,t}(0)\right| e^{-\alpha t}, \quad E_{fc,t} = i_{fc,t} - i_{fc,d} \tag{10}$$

Our control objective is to stabilize the origin $E_s = E_{fc} = 0$ in the presence of the exogenous input i_L with the aforementioned design of $i_{fc,d}$ and i_{uc} in Eqs.(6) and (8) respectively. In this section, we adopt a Lyapunov-based approach to develop a robust nonlinear control strategy. We first observe from *Converse Lyapunov Theorems*, [11], that since $E_{fc,t}$ has an exponentially stable behavior, there exists a positive definite function $\bar{V}_{fc}$ such that,

$$\alpha_1 E_{fc,t}^2 \leq \bar{V}_{fc}(E_{fc,t}) \leq \alpha_2 E_{fc,t}^2, \text{ and } \dot{\bar{V}}_{fc} \leq -\alpha_3 E_{fc,t}^2,\ \alpha_3 > 0 \tag{11}$$

where $0 < \alpha_1 < \alpha_2$. We use the Lyapunov function candidate

$$\bar{V} = \frac{1}{2}E_s^2 + \bar{V}_{fc} + \frac{1}{2}E_{fc}^2 \tag{12}$$

Next, we consider the following dynamical equation of the ultra-capacitor,

$$\dot{V}_{uc} = -\frac{i_{uc}}{C} \Rightarrow \dot{E}_s = -\frac{i_{uc}}{V_{max}} \tag{13}$$

From Eqs.(5), (6), (8) and (10) noting that

$$E_{fc} = i_{fc} - i_{fc,t},\ E_{fc,t} = i_{fc,t} - i_{fc,d} \Rightarrow i_{fc} = E_{fc} + E_{fc,t} + i_{fc,d}$$

we have,

$$\begin{aligned}
\dot{E}_s &= -(1/CV_{max})\left[(V_L i_L/\eta_2 V_{uc})\right. \\
&\quad \left. -\left(\eta_1 V_{fc}/\eta_2 V_{uc}\right)\left(E_{fc} + E_{fc,t} + i_{fc,d}\right)\right] \\
&= -(1/CV_{max})\left[(V_L i_L/\eta_2 V_{uc})\right. \\
&\quad -\left(\eta_1 V_{fc}/\eta_2 V_{uc}\right)\left\{E_{fc} + E_{fc,t} + \left(V_L i_L \bar{\eta}_1 V_{fc}\right)\right. \\
&\quad \left.\left. +g(E_s) + \delta_1\right\}\right]
\end{aligned}$$

We now design the compensator $g(E_s)$ as

$$g(E_s) = -k_s E_s, \quad k_s > 0 \tag{14}$$

Thus,

$$\begin{aligned}
\dot{E}_s &= -(1/CV_{max})\left[(V_L i_L/\eta_2 V_{uc}) - \left(\eta_1 V_{fc}/\eta_2 V_{uc}\right)\right. \\
&\quad \left.\left\{E_{fc} + E_{fc,t} + \left(V_L i_L \bar{\eta}_1 V_{fc}\right) + k_s E_s + \delta_1\right\}\right]
\end{aligned} \tag{15}$$

Next, note from Eqs.(5) and (8) that

$$V_L i_L = \eta_1 V_{fc} I_{fc} + \eta_2 V_{uc}\left[\frac{V_L i_L - \bar{\eta}_1 V_{fc} i_{fc,t}}{\bar{\eta}_2 V_{uc}} + h(E_{fc}) + \delta_2\right] \tag{16}$$

We now design the function $h(E_{fc})$ as follows

$$h(E_{fc}) = k_p E_{fc} + k_d \dot{E}_{fc}, \quad k_p, k_d > 0 \tag{17}$$

Combining Eqs.(16) and (17), we have

$$\dot{E}_{fc} = -\alpha E_{fc} + \frac{\beta - \delta_2}{k_d} \tag{18}$$

where,

$$\begin{aligned}
\alpha &= \left[k_p/k_d + \left(V_{fc}/k_d V_{uc}\right)\left(\bar{\eta}_1/\bar{\eta}_2\right)\right] \\
\beta &= (1/\eta_2 V_{uc})\left[V_L i_L(1 - \eta_2/\bar{\eta}_2)\right. \\
&\quad \left. -\eta_1 V_{fc} i_{fc}\left\{1 - (i_{fc,t}/i_{fc})(\bar{\eta}_1/\eta_1)(\eta_2/\bar{\eta}_2)\right\}\right]
\end{aligned}$$

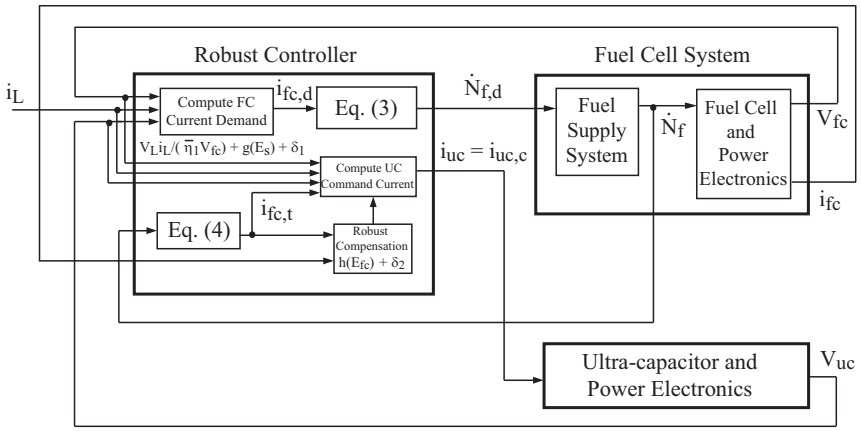

Fig. 7. Nonlinear Control Approach

From Eqs.(11), (12), (15) and (18), we have,

$$\begin{aligned}\dot{\hat{V}} \quad &\leq \quad -\mathscr{E}^T Q \mathscr{E} + \tfrac{E_s}{CV_{max}\eta_2 V_{uc}} \left[\eta_1 V_{fc}\delta_1 - V_L i_L (1 - \tfrac{\eta_1}{\bar{\eta}_1})\right] \\ &\quad + \tfrac{E_{fc}}{k_d}(\beta - \delta_2)\end{aligned} \tag{19}$$

where,

$$\mathscr{E} = \begin{bmatrix} E_s \\ E_{fc,t} \\ E_{fc} \end{bmatrix}, \quad Q = m \begin{bmatrix} k_s & -0.5 & -0.5 \\ -0.5 & \alpha_3/m & 0 \\ -0.5 & 0 & \alpha/m \end{bmatrix}, \tag{20}$$

and $m = \eta_1 V_{fc}/CV_{max}\eta_2 V_{uc}$. Note in Eq.(20), that Q is symmetric. Furthermore, $m > 0$ and has finite positive upper and lower bounds over the range of operation. Among the positive constants k_s, α and α_3, note that α_3 is not a tunable parameter since it is determined by the characteristics of the fuel supply system. However, by choosing k_s and α appropriately, we can ensure $Q > 0$ for all feasible values of m. Thus, from the *Rayleigh-Ritz Inequality*, we have

$$\mathscr{E}^T Q \mathscr{E} \geq \inf(\lambda_{min,Q})\,||\mathscr{E}||^2 > 0 \quad \forall\, \mathscr{E} \neq 0 \tag{21}$$

where $\lambda_{min,Q}$ represents the smallest eigenvalue of Q at any instant. Furthermore, note that by choosing δ_1 and δ_2 as

$$\delta_1 \begin{cases} \leq & \left(V_L i_L/\eta_1 V_{fc}\right)(1 - \eta_1/\bar{\eta}_1) \quad \text{for} \quad E_s > 0 \\ \geq & \left(V_L i_L/\eta_1 V_{fc}\right)(1 - \eta_1/\bar{\eta}_1) \quad \text{for} \quad E_s \leq 0 \end{cases} \tag{22}$$

and

$$\delta_2 \begin{cases} \geq & \beta \quad \text{for} \quad E_{fc} > 0 \\ \leq & \beta \quad \text{for} \quad E_{fc} \leq 0 \end{cases} \tag{23}$$

we have from Eqs.(19) and (21)

$$\dot{\hat{V}} \leq -\mathscr{E}^T Q \mathscr{E} \leq \inf(\lambda_{min,Q})\,||\mathscr{E}||^2 < 0, \quad \forall\, \mathscr{E} \neq 0 \tag{24}$$

Note that the conditions in Eqs.(22) and (23) are implementable since E_s, E_{fc}, and all voltage and current variables are measurable. Also, upper and lower bounds of η_1 and η_2 can be estimated. From Eqs.(11), (12) and (24), we conclude that the control design in Eqs.(6) and (8), with $g(E_s)$, $h(E_{fc})$ designed as in Eqs.(14) and (17) respectively, and δ_1, δ_2 chosen as in Eqs.(22) and (23) respectively, guarantee *exponential stability* of the origin $\mathscr{E} = 0$. It is noted that the exponential stability condition in Eq.(9) can be relaxed. For instance, if the fuel supply dynamics is simply *Input-to-State Stable, ISS* [11], we can show that the origin $\mathscr{E} = 0$ will also satisfy the *ISS* property. We omit this proof for conciseness.

B. H_∞ Control

In this section, we design an alternate control scheme incorporating an H_∞ based approach [15]. Referring to Fig.7 and Eq.(6), the only difference introduced by the H_∞ approach compared to the nonlinear control in section VI-A is that $i_{fc,d}$ is computed as

$$i_{fc,d} = \frac{V_L i_L}{\bar{\eta}_1 V_{fc}} + \delta_{i_{fc}} \tag{25}$$

where, $\delta_{i_{fc}}$ is obtained through an H_∞ synthesis. A state space representation of the system is needed to perform the H_∞ control synthesis where all uncertainties and disturbances are included. From Eqs.(5) and (13), we have

$$\dot{V}_{uc} = \frac{1}{CV_{uc}\eta_2}[V_L i_L - \eta_1 V_{fc} i_{fc}] \tag{26}$$

Expressing i_{fc} as

$$i_{fc} = i_{fc,d} + \sigma \tag{27}$$

where σ represents a bounded unknown error term, we get from Eqs.(25), (26) and (27),

$$\dot{V}_{uc} = \frac{1}{CV_{uc}\eta_2}\left[V_L i_L \left(1 - \frac{\eta_1}{\bar{\eta}_1}\right) - V_{fc}\eta_1(\delta_{i_{fc}} + \sigma)\right] \tag{28}$$

Eq.(28) can be expressed as

$$\dot{V}_{uc} = f - g(\delta_{i_{fc}} + \sigma),\; f = \frac{V_L i_L}{CV_{uc}\eta_2}\left(1 - \frac{\eta_1}{\bar{\eta}_1}\right),\; g = \frac{V_{fc}\eta_1}{CV_{uc}\eta_2} \tag{29}$$

We design $\delta_{i_{fc}}$ as follows,

$$\delta_{i_{fc}} = \frac{1}{\hat{g}}\left(\hat{f} - v\right) \quad \Rightarrow \quad i_{fc,d} = \frac{V_L i_L}{\bar{\eta}_1 V_{fc}} + \frac{1}{\hat{g}}\left(\hat{f} - v\right) \tag{30}$$

where $\hat{f}$ and $\hat{g}$ are the estimates of the functions f and g respectively, evaluated with nominal values. In the H_∞ control design, we evaluate the maximum bounds of deviation by evaluating f and g with maximum upper and minimum lower

bounds possible for all uncertain and variable quantities. Substituting for $\delta_{i_{fc}}$ from Eq.(30) into Eq.(29), we get

$$\dot{V}_{uc} = \frac{g}{\hat{g}} v + \left[f - \frac{g}{\hat{g}} \hat{f} - g\sigma \right] \tag{31}$$

Representing $g/\hat{g}$ as a nominal value β_0 plus maximum deviation $\Delta\beta_0$, and assigning the rest of Eq.(31) as disturbances d, we have

$$\dot{V}_{uc} = (\beta_0 + \Delta\beta) v + d \tag{32}$$

where, the modified control input v is computed using the dynamic feedback law

$$v(s) = K_\infty(s)\, e(s), \quad e(t) = V_{uc,t} - V_{uc} \tag{33}$$

where K_∞ is a time-varying gain obtained using standard H_∞ synthesis and $V_{uc,t}$ is the target ultra-capacitor voltage that results in the target SOC, S_t. The H_∞ synthesis is carried out using MATLAB®'s robust control toolbox. As mentioned at the beginning of this section, referring to Fig.7, the H_∞ approach only introduces a modification to the calculation of $i_{fc,d}$, given by Eq.(30).

VII. Experimental Test-Stand

We test the control strategy design developed in sections VI-A and VI-B on an experimental test-stand, shown in Fig. 8. The test-stand consists of

Fuel Cell Emulator: An SOFC system is emulated by executing a detailed mathematical model on a dSPACE® DS1103 real time processor in conjunction with a $100V/50A$ programmable power supply. A schematic diagram of the emulator is shown in Fig.9.

Electronic Load: A DC electronic load, shown in Fig.8, is used for power consumption. The load can draw a maximum power of 1.8kW with a maximum voltage of 60V and a maximum current of 120A.

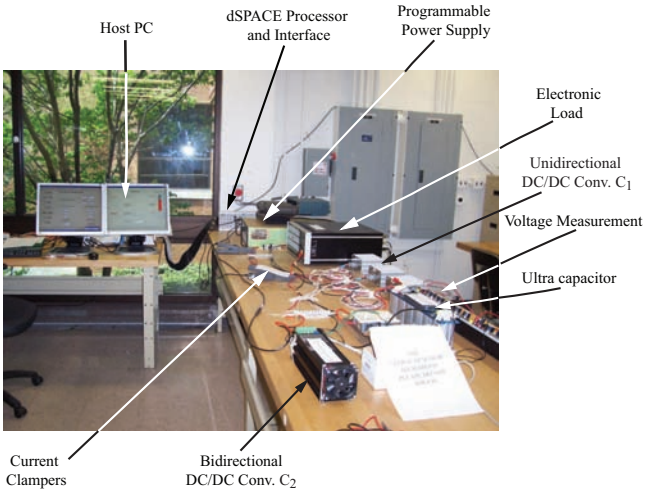

Fig. 8. Experimental Test Stand

Unidirectional DC/DC Converter: A unidirectional DC/DC converter, denoted by C_1 in Fig 9, provides a uniform 24V voltage V_L at the output, with a maximum current rating of 33A.

Voltage Measurement: The voltage of the ultra-capacitor is measured at all times using voltage probes with high input impedance, as shown in Fig. 8.

Ultra-capacitor: A 16V series BMOD0250-E016 ultra-capacitor from MAXWELL Technologies is used in this experimental set up. The specifications are: $C = 250$F, $V_{max} = 16.2$V, and internal resistance is ≈ 4.1mΩ.

Bidirectional DC/DC Converter: A bidirectional DC/DC Converter, denoted by C_2 in Fig.9, is used to command the ultra-capacitor current i_{uc}. The converter has two control mode capabilities, current control mode or voltage control mode. We use the current control mode in our application.

Current Clampers: Measurement for i_L and i_{fc} are obtained using Fluke 80i-110s AC/DC current probes.

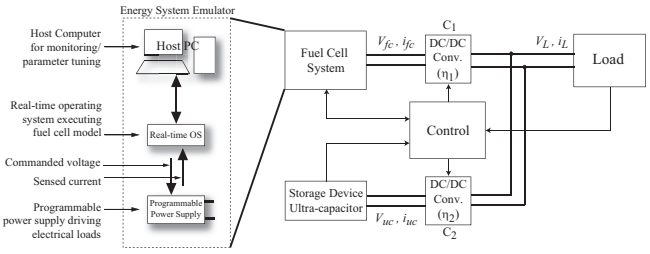

Fig. 9. Fuel Cell Emulator within Hybrid Energy System

VIII. Experimental Results

We present results of experiments carried out on the test stand described in section VII. Application of nonlinear and H_∞ control is shown. In all tests, we emulate an SOFC system with $\mathcal{N}_{cell} = 50$ connected in series. The fuel supply is assumed to follow a first order dynamics with $\dot{N}_f(s) = [1/(2s+1)]\dot{N}_{f,d}(s)$. Neither control designs assume knowledge of this dynamics. The bus voltage is $V_L = 24$V and the ultra-capacitor specifications are $C = 250$F and $V_{max} = 16.2$V. Other salient aspects of the hybrid system, mentioned in section V, are also applicable for all experiments.

A. Nonlinear Control

In this section, we present results of the nonlinear control strategy developed in section 7. The results are presented in Fig.10. The following control parameters were chosen: $U_{ss} = 0.8$, $S_t = 0.8$, $\bar{\eta}_1 = 1$, $\bar{\eta}_2 = 0.98$, $k_s = 0.1$, $k_p = 0.2$, and $k_d = 0.004$. The terms δ_1 and δ_2 were chosen based on Eqs.(22) and (23), as follows:

$$\delta_1 = \begin{cases} 0 & \text{for} \quad E_s > 0 \\ 2 & \text{for} \quad E_s \le 0 \end{cases}, \quad \delta_2 = \begin{cases} 2 & \text{for} \quad E_{fc} > 0 \\ -2 & \text{for} \quad E_{fc} \le 0 \end{cases}$$

In Fig.10, i_L is subject to step changes, as shown in Fig.10(a). The corresponding variations in i_{fc}, V_{fc}, U and $\dot{N}_f$ are plotted in Figs.10(b), (c), (d) and (e) respectively. In Fig.10(b), both i_{fc} and $i_{fc,t}$ are plotted together but are indistinguishable as they coincide at most instants. The ultra-capacitor SOC and current i_{uc} are plotted in Figs.10(f) and (g) respectively, and the fuel cell and ultra-capacitor powers are plotted together in Fig.10(h). The results show close control of U in spite of drastic transients in i_L. Fig.10(f) shows tight control of S around the target value of 0.8.

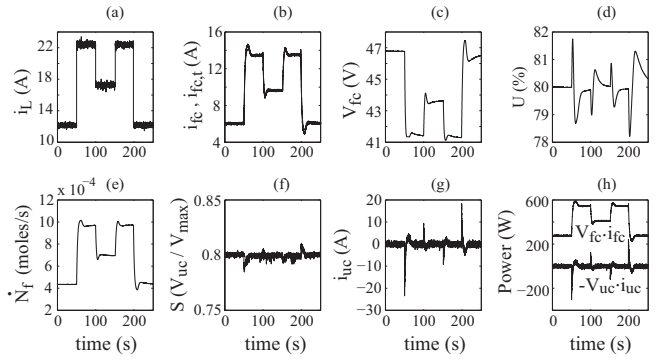

Fig. 10. Nonlinear Control under Transient i_L

B. H_∞ Control

In this section, we present results of the H_∞ control developed in section VI-B. The results are presented in Fig.11. The following control parameters were chosen: $U_{ss} = 0.8$, $S_t = 0.8$, $k_p = 0.2$, and $k_d = 0.004$. The following ranges were chosen for uncertain quantities with nominal values at the middle of the respective ranges: $\bar{\eta}_1, \bar{\eta}_2 \in [0.8\ 1]$, $V_{fc} \in [40\ 60]$V and $V_{uc} \in [9.6\ 16.2]$V. Referring to Eq.(33), H_∞ synthesis yielded the following feedback law

$$K_\infty = \frac{v(s)}{e(s)} = \frac{3.587 \times 10^4 s + 1.75 \times 10^4}{s^2 + 1049s + 105.4}$$

In Fig.11, i_L undergoes the same transients as in Fig.10. Figs.10 and 11 indicate comparable performance of the

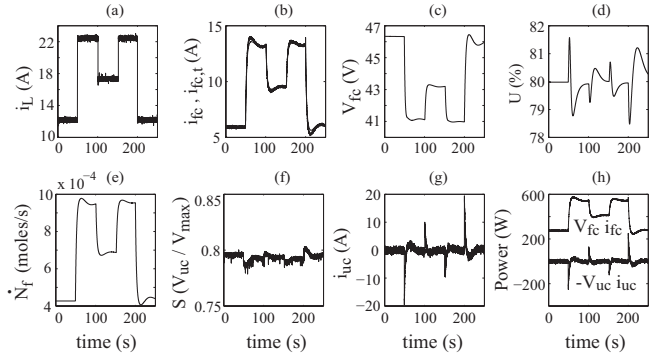

Fig. 11. H_∞ Control under Transient i_L

H_∞ and the nonlinear control strategy. The only noticeable difference is in the SOC control, Figs.10(f) and 11(f), where the nonlinear control seems to perform slightly better.

IX. CONCLUSION

We address the control of a hybrid SOFC ultra-capacitor system. The proposed control designs are based on regulating the power draw from the fuel cell and using an ultra-capacitor for compensating the excess or deficit power during transients. Two control designs are proposed. The first is a robust nonlinear control strategy and the second is a standard H_∞ approach. Both address multiple objectives; minimizing transient deviation in U from a target, and maintaining a constant ultra-capacitor SOC. An experimental test-stand is developed, consisting of an emulated SOFC and actual ultra-capacitor and power-electronics components, forming a laboratory scale hybrid power grid. Both control strategies show comparable performance on this platform. In our future research, conditions which are more likely to occur in higher power systems such as saturated fuel flow, limiting fuel cell current density, limiting ultra-capacitor current, will be considered. In such cases, addition of a battery is foreseen.

REFERENCES

[1] M. Y. Ayad, M. Becherif, A. Djerdir, and A. Miraoui. Sliding mode control for energy management of dc hybrid power sources using fuel cell, batteries and supercapacitors. *International Conference on Clean Electrical Power*, pages 500–505, 2007.

[2] T. Das. An adaptive observer design for recirculation based solid oxide fuel cell systems using cell voltage measurement. *American Control Conference, St. Louis, MO.*, 2009.

[3] T. Das, S. Narayanan, and R. Mukherjee. Model based characterization of transient response of a solid oxide fuel cell system. *ASME International Mechanical Engineering Congress and Exposition*, pages 655–664, 2007.

[4] T. Das and R. Weisman. A feedback based load shaping strategy for fuel utilization control in sofc systems. *American Control Conference, St. Louis, MO.*, 2009.

[5] A. Drolia, P. Jose, and N. Mohan. An approach to connect ultracapacitor to fuel cell powered electric vehicle and emulating fuel cell electrical characteristics using switched mode converter. *Proceedings of Industrial Electronics Conference*, pages 897–901, 2003.

[6] M. L. Ferrari, A. Traverso, L. Magistri, and A. F. Massardo. Influence of anodic recirculation transient behavior on the SOFC hybrid system performance. *Journal of Power Sources*, 149:22–32, 2005.

[7] E. M. Fleming and I. A. Hiskens. Dynamics of a microgrid supplied by solid oxide fuel cells. *iREP Symposium - Bulk Power System Dynamics and Control - VII, Charleston, SC*, 2007.

[8] A. Hajizadeh and M. A. Golkar. Intelligent power management strategy of hybrid distributed generation systems. *Electrical Power and Energy Systems*, 29:783–795, 2007.

[9] Z. Jiang, L. Gao, and R. A. Dougal. Adaptive control strategy for active power sharing in hybrid fuel cell/battery power sources. *IEEE Transactions on Energy Conversion*, 22(2):507–515, 2007.

[10] R. Kandepu, L. Imsland, B. A. Foss, C. Stiller, B. Thorud, and O. Bolland. Modeling and control of a SOFC-GT-based autonomous power system. *Energy*, 32:406–417, 2007.

[11] H. Khalil. *Nonlinear Systems*. Prentice-Hall, Inc. Upper Saddle River, NJ, 3 edition, 2002.

[12] A. Lazzaretto, A. Toffolo, and F. Zanon. Parameter setting for a tubular SOFC simulation model. *ASME Journal of Energy Resources Technology*, 126:40–46, 2004.

[13] F. Mueller, J. Brouwer, F. Jabbari, and S. Samuelsen. Dynamic simulation of an integrated solid oxide fuel cell system including current-based fuel flow control. *ASME Journal of Fuel Cell Science and Technology*, 3:144–154, 2006.

[14] V. Paladini, T. Donateo, A. de Risi, and D. Laforgia. Super-capacitor fuel-cell hybrid electric vehicle optimization and control strategy development. *Energy Conversion and Management*, 48:3001–3008, 2007.

[15] S. Skogestad and I. Postlethwaite. *Multivariable Feedback Control: Analysis and Design*. John Wiley & Sons, Ltd., 2 edition, 2005.

[16] J. Sun and I. Kolmanovsky. Load governor for fuel cell oxygen starvation protection: A robust nonlinear reference governor approach. *Proceeding of the 2004 American Control Conference, Boston, MA June 30 - July 2*, pages 828–833, 2004.

[17] P. Thounthong, S. Rael, and B. Davat. Control strategy of fuel cell/supercapacitors hybrid power sources for electric vehicle. *Journal of Power Sources*, 158:806–814, 2006.

[18] M. Uzunoglu and M. S. Alam. Dynamic modeling, design and simulation of a pem fuel cell/ultracapacitor hybrid system for vehicular applications. *Energy Conversion and Management*, 48:1544–1553, 2007.

[19] A. Vahidi, A. Stefanopoulou, and H. Peng. Current management in a hybrid fuel cell power system: A model-predictive control approach. *IEEE Transactions on Control Systems Technology*, 14(6):1047 – 1057, 2006.